Pharmaceutical Research, Vol. 25, No. 8, August 2008 (© 2008)
DOI: 10.1007/s11095-008-9600-9

Research Paper

Selective Contrast Enhancement of Individual Alzheimer's Disease Amyloid Plaques Using a Polyamine and Gd-DOTA Conjugated Antibody Fragment Against Fibrillar Aβ42 for Magnetic Resonance Molecular Imaging

Muthu Ramakrishnan,[1] Thomas M. Wengenack,[1] Karunya K. Kandimalla,[1,2] Geoffry L. Curran,[1] Emily J. Gilles,[1] Marina Ramirez-Alvarado,[3] Joseph Lin,[4] Michael Garwood,[4] Clifford R. Jack Jr.,[5] and Joseph F. Poduslo[1,3,6]

Received January 22, 2008; accepted April 10, 2008; published online April 29, 2008

Purpose. The lack of an *in vivo* diagnostic test for AD has prompted the targeting of amyloid plaques with diagnostic imaging probes. We describe the development of a contrast agent (CA) for magnetic resonance microimaging that utilizes the $F(ab')_2$ fragment of a monoclonal antibody raised against fibrillar human Aβ42

Methods. This fragment is polyamine modified to enhance its BBB permeability and its ability to bind to amyloid plaques. It is also conjugated with a chelator and gadolinium for subsequent imaging of individual amyloid plaques

Results. Pharmacokinetic studies demonstrated this ^{125}I-CA has higher BBB permeability and lower accumulation in the liver and kidney than $F(ab')_2$ in WT mice. The CA retains its ability to bind Aβ40/42 monomers/fibrils and also binds to amyloid plaques in sections of AD mouse brain. Intravenous injection of ^{125}I-CA into the AD mouse demonstrates targeting of amyloid plaques throughout the cortex/hippocampus as detected by emulsion autoradiography. Incubation of AD mouse brain slices *in vitro* with this CA resulted in selective enhancement on T_1-weighted spin-echo images, which co-register with individual plaques observed on spatially matched T_2-weighted spin-echo image

Conclusions. Development of such a molecular probe is expected to open new avenues for the diagnosis of AD.

KEY WORDS: Alzheimer's disease; amyloid plaques; antibody fragments; contrast agent; magnetic resonance imaging.

INTRODUCTION

Alzheimer's disease (AD) is an incurable neurodegenerative disease characterized pathologically by the extracellular deposition of amyloid plaques and the intracellular formation of neurofibrillary tangles (1). There is currently no *in vivo* diagnostic technique apart from memory testing, which is mostly limited to advanced AD patients with significant neurodegeneration, and histological examination, which is conducted post-mortem, to definitively diagnose AD. Early detection of AD will be a prerequisite for early intervention and successful treatment of the disease. Targeting the extracellular amyloid plaques with diagnostic imaging probes detectable by different neuroimaging techniques would provide a more definitive pre-mortem diagnosis of AD.

Amyloid plaques have been successfully imaged in living human patients using positron emission tomography (PET) with the use of amyloid-binding radiotracer compounds (2–4). The method, however, is limited by several problems; namely poor spatial resolution with a detection limit of ~2 mm, the inability to visualize individual amyloid plaques, and the need for rapid synthesis and use of PET tracers, which are very short-lived radioisotopes. Magnetic resonance microimaging (MRMI) has an advantage of high spatial resolution and the ability to detect individual amyloid plaques as small as 35 μm in diameter in 9 month old live AD mice (5).

In recent years, two different technical approaches have been taken to image individual amyloid plaques in AD mice using magnetic resonance imaging (MRI). One approach is to use exogenous plaque binding contrast agents (6,7). In the study by Poduslo et al. (6), whole AD mice brains were imaged *ex vivo* and individual amyloid plaques were identified after intravenous administration of an exogenous plaque labeling contrast agent. Another approach is to image individual amyloid plaques without any contrast agent

[1] Molecular Neurobiology Laboratory, Departments of Neurology and Neuroscience, Mayo Clinic College of Medicine, 200 First Street SW, Rochester, Minnesota 55905, USA.
[2] College of Pharmacy and Pharmaceutical Sciences, Florida A&M University, Tallahassee, Florida, USA.
[3] Department of Biochemistry and Molecular Biology, Mayo Clinic College of Medicine, Rochester, Minnesota, USA.
[4] Center for Magnetic Resonance Research and Department of Radiology, University of Minnesota, Minneapolis, Minnesota, USA.
[5] Department of Radiology, Mayo Clinic College of Medicine, Rochester, Minnesota, USA.
[6] To whom correspondence should be addressed. (e-mail: poduslo.joseph@mayo.edu)

utilizing the endogenous iron content present in the amyloid plaques (5,6,8–11).

The presence of the blood brain barrier (BBB) hinders the delivery of macromolecules into the brain unless their uptake is receptor mediated. Immunoglobulins (IgG) are large heterotetrameric protein complexes restricted to slow passive diffusion or fluid phase endocytosis. The permeability coefficient×surface area product (PS) of IgG at the BBB is $\sim 0.1 \times 10^{-6}$ ml g^{-1} s^{-1}, which is about 240-fold less than the PS values of insulin which is known to undergo receptor-mediated transport at the BBB (12,13). Several strategies were developed in the past couple of decades to deliver macromolecules to the brain. Some of these strategies include: (1) "piggy-backing" macromolecules with low permeability to ligands that have significant receptor mediated transcytosis across the BBB; (2) modifying the macromolecules with polyamine to increase their permeability at the BBB; and (3) temporary opening of the BBB by administering hyperosmotic solutions of mannitol. Due to the invasive nature of the third approach, more efforts have focused on the first two approaches. Our laboratory has focused on increasing the BBB permeability of macromolecules via polyamine modification. We have demonstrated that the covalent attachment of naturally occurring polyamines, such as putrescine, to proteins significantly increases their permeability at the BBB without significantly affecting their biological activity (13).

Recently, our group reported that a polyamine modified $F(ab')_2$ 4.1 antibody fragment of a monoclonal antibody, IgG4.1, raised against the fibrillar human amyloid protein Aβ42 showed increased BBB permeability with retained antigen binding ability to Aβ peptides and amyloid plaques under *in vitro* conditions (14). Moreover, radioiodinated pF$(ab')_2$4.1 labeled amyloid deposits in AD transgenic mouse brain following intravenous (IV) injection as detected by emulsion autoradiography. Coupling of appropriate contrast agents to pF$(ab')_2$4.1 might facilitate the molecular imaging of amyloid deposits using MRI. Here we report the development of a novel contrast agent, Gd-DOTA-pF$(ab')_2$4.1, with a covalently attached contrast agent moiety (Gd-DOTA) for development as a potential plaque specific contrast agent for the *in vivo* diagnosis of AD.

MATERIALS AND METHODS

Animals. The *in vivo* labeling experiments were performed using transgenic mice that express two mutant human proteins associated with familial AD and have been described in detail elsewhere (15). Hemizygous transgenic mice (Tg2576) expressing mutant human amyloid precursor protein (APP_{695}) (16) were mated with a strain of homozygous transgenic mice (M146L6.2) expressing mutant human presenilin 1 (PS1) (15). In one experiment, an APP (Tg2576) mouse was used. The animals were genotyped for the expression of both transgenes by a PCR method using a sample of mouse-tail DNA. The mice were housed in a virus-free barrier facility under a 12-h light/dark cycle, with ad libitum access to food and water. All procedures performed were in accordance with NIH Guidelines for the Care and Use of Laboratory Animals using protocols approved by the Mayo Institutional Animal Care and Use Committee.

Preparation of $F(ab')_2$4.1 fragments. Monoclonal IgG4.1 was developed as described by Poduslo et al. (14). It is a monoclonal antibody that binds to the first 15 amino acid residues of soluble and fibrillar Aβ40/42 peptides (unpublished results). Pure $F(ab')_2$4.1 was obtained by digesting IgG4.1 using ficin at pH 6.5. The purification of the $F(ab')_2$4.1 from the digested sample was followed as described previously by Poduslo et al. (14). Sample purity was evaluated by 7.5% SDS-PAGE, and protein concentrations were determined using the BCA protein assay (Pierce Biotechnology).

Conjugation of DOTA to $F(ab')_2$4.1. The chelating agent 1,4,7,10-tetra-azacyclododecane-1,4,7,10-tetraacetic acid (DOTA; Strem Chemicals, Newburyport, MA), was coupled to $F(ab')_2$4.1 using the carbodiimide reaction as described by Smith-Jones and Solita (17). DOTA was preferred over diethylenetriaminepentaacetate (DTPA) as the chelating agent due to the higher stability of its gadolinium complex. Conjugation of DOTA to $F(ab')_2$4.1 involved two steps. In the first step, the active ester of DOTA was generated with carbodiimide at pH 7.8. In the second step, the active ester reacted with the amine side chain functional groups of lysine present in $F(ab')_2$4.1. The number of DOTA molecules attached to $F(ab')_2$4.1 was controlled by changing the aliquot concentration of the added active ester, by adjusting the reaction time and controlling the pH. Initially, the reactions were performed by mixing 1 mg of pure $F(ab')_2$4.1 with 80 μl of freshly prepared active ester, which is prepared using 0.361 mmol of DOTA and 0.313 mmol of *N*-hydroxy succinimide in 2 ml of metal free distilled water at pH 6.8 as described in Smith Jones and Solita (17), for different time periods (0.5, 1, 2, 18 h) at room temperature. For the characterization of DOTA-$F(ab')_2$4.1 conjugate, the reaction mixture was concentrated using a 30kDa MWCO centrifugal filter (Vivaspin 20, Vivascience Sartorius group, Hannover, Germany) to about 5 mg/ml and washed (at least 12 times) with equal volumes of 1 M ammonium acetate (metal free) at pH 6.8. The success of this coupling was evaluated by incubating this derivative with an equimolar amount of radioactive gadolinium (^{153}Gd) for subsequent autoradiographic analysis following SDS-PAGE. For the preparation of contrast agent for all other experiments, 1 mg of $F(ab')_2$4.1 was mixed with 120 μl of fresh active ester and incubated at room temperature for 0.5 h and non-radioactive $GdCl_3$ was used for chelation. The Gd-DOTA-$F(ab')_2$4.1 was further modified with the polyamine, putrescine using the carbodiimide reaction as described previously (14).

SDS-Polyacrylamide Gel Electrophoresis (SDS-PAGE) and Isoelectric Focusing (IEF). Aliquots of IgG4.1, pF$(ab')_2$4.1, and Gd-DOTA-pF$(ab')_2$4.1 were run on a SDS-PAGE gel (7.5% *T* and 1% *C*) in the absence of a reducing agent and stained with Coomassie blue using standard methods (18). IEF of IgG4.1 and pIgG4.1 as well as the $F(ab')_2$4.1 and pF$(ab')_2$4.1 samples were performed using a Bio-Rad Model 111 Mini IEF Cell according to the manufacturer's instructions. Briefly, 40% Bio-Lyte 3/10 ampholyte solution (Bio-Rad, Hercules, California) was used with a polyacrylamide gel (25% *T*, 0.75% *C*). The gels were cast between the acrylic casting tray and gel support film to give a gel dimensions of 125×65×0.4 mm. Monomer ampholyte poly-

merization time under a fluorescent desk lamp was 45 min. Samples were loaded and allowed to diffuse into the gel for 6 min. IEF was carried out under constant voltage in a stepped fashion: 45 min at 100 V and 15 min at 450 V. Bio-Rad IEF standards containing nine native proteins with isoelectric points ranging from 4.45 to 9.6, as well as albumin (4.7) and cytochrome C (9.6), were run for comparison. All bands were visualized with 0.04% Coomassie Brilliant Blue stain.

Estimation of Bound DOTA per F(ab′)$_2$4.1 Molecule by Paper Chromatography. Three 20 μl aliquots from 10 mg/ml DOTA-F(ab′)$_2$4.1 conjugates were mixed with 10, 20, 30 μl aliquots of 1 mM $GdCl_3$ spiked with a trace amount of radioactive ^{153}Gd. The mixtures were incubated at 37°C for 16 h and then reincubated at 37°C for another 5 h after the addition of 50 μl of 5 mM DTPA. Five μl of sample was spotted onto a 20 cm silica gel impregnated glass fiber chromatography strip (Gelman Sciences, Ann Arbor, MI) and eluted with 5 mM DTPA (pH 6.0). The relative amount of bound Gd per molecule of DOTA-F(ab′)$_2$4.1 was determined by cutting the strip to 1 cm wide pieces and counting each of them in a gamma counter. Conjugated Gd-DOTA-F(ab′)$_2$4.1 remained at the origin whereas free (Gd-DTPA) moved with the solvent front.

The number of DOTA covalently linked per F(ab′)$_2$4.1 molecule (N) was calculated from the mole ratio between Gd and DOTA-F(ab′)$_2$4.1 and from the observed ratio of [Gd-DOTA-F(ab′)$_2$4.1] and [Gd-DTPA]:

$$N = \frac{\text{Radioactivity at origin (cpm)} \times \text{Gd mole concentration}}{\text{Total radioactivity (cpm)} \times \text{Antibody fragment mole concentration}}$$

The Gd concentration was further quantified using the mass spectroscopic facility at the University of California, Los Angels using Agilent 7500CC quadrupole inductively coupled mass spectrometer (ICP-MS).

Plasma Pharmacokinetic Studies. After catheterizing the femoral vein and the femoral artery of each mouse under general anesthesia (isoflurane=1.5%; oxygen=4 l/min), ^{125}I-F(ab′)$_2$4.1 or ^{125}I-Gd-DOTA-pF(ab′)$_2$4.1 were administered intravenously in the femoral vein. The plasma pharmacokinetics of these compounds were determined by collecting serial blood samples (20 μl) from the femoral artery over a period of time. The blood samples were diluted to a volume of 100 μl with normal saline, centrifuged, and the supernatant was obtained. TCA precipitation was conducted and the supernatants of the samples and the pellets were assayed for ^{125}I radioactivity in a gamma counter (Cobra II, Packard).

Plasma pharmacokinetic parameters of ^{125}I-F(ab′)$_2$4.1 and ^{125}I-Gd-DOTA-pF(ab′)$_2$4.1 were estimated by nonlinear curve fitting of the experimental data using Gauss-Newton (Levenberg and Hartley) algorithm (WinNonlin® Professional, version 5.2, Mountain view, CA). Secondary parameters such as the C_{max} (maximum plasma concentration), the plasma clearance (CL), volume of distribution, and area under the plasma concentration curve (AUC) were also calculated using the WinNonlin® software. The mean parameter values of both compounds were compared by Student's t-test using GraphPad Prism version 4.0 (GraphPad Software, San Diego, CA).

Permeability Measurements of Radioiodinated F(ab′)$_2$4.1, pF(ab′)$_2$4.1 and Gd-DOTA-pF(ab′)$_2$4.1 at the BBB. Aliquots of the proteins were labeled with ^{125}I using the chloramine-T procedure and PS/V_p (PS: permeability coefficientsurface area product—in $\times 10^{-6}$ milliliters per gram per second; V_p: residual brain region blood volume in microliters per gram) measurements were performed as described previously (12,19). Further discussions about the PS and V_p terms can be found in Bassingthwaighte et al. (20). Briefly, an IV bolus injection of phosphate-buffered saline, pH 7.4 (PBS) containing either ^{125}I-F(ab′)$_2$4.1, ^{125}I-pF(ab′)$_2$4.1, or ^{125}I-Gd-DOTA-pF(ab′)$_2$4.1 (100 μCi) was rapidly injected into the femoral vein of an anesthetized (isoflurane, 1.5%) WT mouse. Serial blood samples (20 μl) were collected from the femoral artery over the next 30–120 min, diluted to a volume of 100 μl with saline, and centrifuged. The supernatant was then TCA precipitated, and the precipitate was assayed for ^{125}I radioactivity. At 30–60 s prior to the end of the experiment, a aliquot of ^{131}I radiolabeled bovine serum albumin (100 μCi) was administered IV to serve as a V_p indicator of vascular space. After the final blood sample, the animals were sacrificed, the brain and meninges were removed, and the brain was dissected into cortex, caudate-putamen (neostriatum), hippocampus, thalamus, brain stem, and cerebellum. Tissue was lyophilized, and dry weights were determined with a microbalance and converted to respective wet weights with wet weight/dry weight ratios previously determined. Tissue and plasma samples were assayed for ^{125}I radioactivity in a two channel gamma counter (Packard COBRA II) with radioactivity corrected for background and crossover of ^{131}I activity into the ^{125}I channel. Data are presented as ±SEM values with statistical evaluation using ANOVA with a significance accepted at the $P<0.05$ level. The PS and V_p measurements were calculated as described previously (21).

Enzyme-Linked Immunosorbent Assay (ELISA). Aβ peptide (Aβ40, Aβ42, and fibrillar Aβ40 and Aβ42) was coated in the wells of 96-well microtiter plates (Immulon 1B, Thermo Lab Systems, Franklin, MA) at a concentration of 1 μg/well. Fibrils were formed by incubating Aβ40 or Aβ42 in pH 7.4 Tris buffer at 37°C for ~48 h. For the soluble form of Aβ peptide, freshly synthesized peptides were used. The wells were washed with PBS and blocked with 100 μl of PBS containing 1% of bovine serum albumin (BSA, Sigma) at room temperature for 60 min. The wells were rinsed again with PBS and serially diluted samples of IgG4G8, IgG4.1, or Gd-DOTA-pF(ab′)$_2$4.1 were then tested in triplicate. The antibody IgG4G8 (Signet Labs, Dedham, MA) was used as a positive control and L227-IgG1 kappa antibody produced by mouse B lymphocyte as a negative control. After 3 h incubation at 37°C, the wells were washed with PBS and incubated with 100 ng of Fab-specific, goat anti-mouse IgG secondary antibody conjugated to alkaline phosphatase (Sigma A-1682) for 1 h at room temperature. The wells were washed and equilibrated with diethanolamine buffer pH 9.8 for 5 min. 4-Nitrophenyl phosphate disodium (pNPP, Sigma) was used as a substrate to visualize the bound antibodies and fragments. After 15 min, the reaction was stopped by adding 50 μl of 1 M sodium hydroxide. Optical densities were recorded at 405 nm using an automated plate reader spectrophotometer (Spectramax Plus).

In Vitro Labeling of Amyloid Plaques in APP/PS1 Mouse Sections with Radioiodinated Antibodies and Fragments. ^{125}I-IgG4.1, ^{125}I-F(ab′)$_2$4.1, ^{125}I-Gd-DOTA-F(ab′)$_2$4.1, ^{125}I-pF(ab′)$_2$4.1, ^{125}I-Gd-DOTA-pF(ab′)$_2$4.1, or buffer were incubated *in vitro* with sections of unfixed APP/PS1 mouse brain using a modified procedure as described previously (22). Free iodine was removed by dialyzing each antibody overnight against PBS and then rinsed further in a centrifugal filter (Vivaspin 20, 30,00 MWCO, Cat. #VS2022, Sartorius AG, Goettingen, Germany) with five changes of PBS. 15 μm cryosections were incubated for 3 h at room temperature with 5×10^5 cpm radioiodinated antibody or in 250 μl of TBS (50 mM Tris HCl, 138 mM sodium chloride, pH 7.0) containing 0.1% BSA, 0.6 mg/ml magnesium chloride, 0.04 mg/ml bacitracin, 0.002 mg/ml chymostatin, and 0.004 mg/ml leupeptin. The sections then underwent immunohistochemistry (IH) for amyloid using an anti-Aβ polyclonal rabbit antibody (Anti-Pan β-Amyloid, 1:2,000, Cat. #44-136, Biosource International, Camarillo, CA). Next, the sections were dipped in an autoradiographic emulsion (Type NTB-3, Kodak, Rochester, NY) for direct comparison of ^{125}I-labeled amyloid deposits to anti-Aβ IH. The slides were dipped in emulsion, exposed for various durations, and developed according to the instructions. The sections were dehydrated with successive changes of ethanol and xylene and then coverslipped.

In Vivo Labeling of Amyloid Plaques in APP/PS1 Mouse Brain with Radioiodinated Antibodies and Fragments. APP/PS1 transgenic mice (9 months of age) were catheterized in the femoral vein under general anesthesia (isoflurane, 1.5%) and injected with 1 mg (2 mCi) of ^{125}I-F(ab′)$_2$4.1, ^{125}I-Gd-DOTA-pF(ab′)$_2$4.1, or a non-specific mouse monoclonal antibody (IgG1 kappa purified from mouse myeloma L227, Cat. #HB-96, ATCC, Manassas, VA) as a control. After 4 h, each animal was given an overdose of sodium pentobarbital (200 mg/kg, IP) and perfused with PBS, followed by neutral-buffered, 10% formalin, and then 10% sucrose, 0.1 M sodium phosphate, pH 7.2. Brains were removed and frozen in 2-methylbutane chilled in dry ice. Frozen sections (15 μm) of each brain were cut with a cryostat and then processed with anti-Aβ IH and emulsion autoradiography for the presence of radiolabeled amyloid deposits using the same methods described above.

Incubation of Gd-DOTA-pF(ab′)$_2$4.1 with APP Mouse Brain Slices In Vitro for MR Imaging of Contrast Enhanced Amyloid Plaques. Gd-DOTA-pF(ab′)$_2$4.1 was incubated with unfixed APP transgenic mouse brain slices to test the ability of Gd-DOTA-pF(ab′)$_2$4.1 to bind amyloid plaques and provide plaque specific contrast enhancement for MRI. Briefly, a 29-month old APP mouse was perfused with PBS following an overdose with sodium pentobarbital (200 mg/kg, IP). The brain was removed and 500-μm slices were cut with a Vibratome. Slices containing the hippocampus were incubated in Gd-DOTA-pF(ab′)$_2$4.1 (1 mg/ml in PBS) for 2 h at 37°C. Control slices were also made by incubating the slices with PBS alone. The slices were rinsed in PBS for 1 h Before fixation, the slices were placed on glass microscope slides under 500-μm coverwells (Grace Bio-Labs, Bend, OR) to keep them flat. The slices were then fixed with neutral-buffered, 10% formalin overnight at 4°C. The next day, the slices were rinsed in PBS for 3 h at 4°C to remove excess formalin. The slices were embedded in 2% agar (Difco Bacto-Agar, Difco Laboratories, Detroit, MI) in a one-well, tissue culture chamber slide (Lab-Tek, Cat. #177410, Nalge Nunc International, Naperville, IL) in a stacked orientation on the slide for MRI. The slices were imaged with a single loop coil using T_1- and T_2-weighted spin echo sequences in a 9.4 *T* horizontal bore scanner. The T_2-weighted spin-echo (T_2SE) imaging parameters were: repetition time (TR)=2,000 ms; echo time (TE)=51.25 ms; image matrix size=25×96×32 in the *x*, *y*, and *z* directions, respectively, at corresponding fields-of-view (FOV) of 15.36×5.76×3.84 mm, which resulted in nominal voxel dimensions of 60×60×120 μm. Acquisition time using the T_2SE sequence was 1 h, 42 min.

The T_1-weighted spin-echo (T_1SE) sequence parameters were: TR=400 ms, TE=7 ms, bandwidth=84 kHz; image matrix size=256×256×32 in the *x*, *y*, and *z* directions, respectively, with a corresponding FOV of 15.36×15.36×3.84 mm. This resulted in nominal voxel dimensions of 60×60×120 μm, respectively. Acquisition time with the T_1SE sequence was 1 h, 8 min for one signal average.

RESULTS

Preparation of the Contrast Agent. Purified F(ab′)$_2$4.1 was successfully linked with a chelating agent DOTA using carbodiimide chemistry at pH 7.8. The success of coupling F(ab′)$_2$4.1 with DOTA was evaluated by incubating DOTA-F(ab′)$_2$4.1 conjugate with equimolar radioactive gadolinium (^{153}Gd) at pH 7.0 for subsequent autoradiographic analysis following SDS-PAGE (Fig. 1A). The autoradiogram showed a band close to 30 kDa which corresponds to the reduced light and heavy chains of Gd-DOTA coupled F(ab′)$_2$4.1. The band intensity increases with increasing reaction time period which indicates increasing amount of DOTA covalently linked with F(ab′)$_2$4.1. The weak band close to 15 kDa likely corresponds to unpurified SDS reduced impurity from the antibody digestion mixture such as Ficin, or more likely Fc fragments that result from the digestion and that are not removed during the purification process.

The number of bound DOTA per F(ab′)$_2$4.1 molecule was calculated using paper chromatography, and the reaction conditions were controlled to covalently link either one or two DOTA per F(ab′)$_2$4.1 molecule by the addition of active ester with a reaction time of 0.5 h Figure 1B shows that the number of bound DOTA per F(ab′)$_2$4.1 ranged between one and three molecules and increases linearly with added active ester in the range studied. Similar results were found when the compounds were analyzed by ICP mass spectral analysis. The linear trend of the curve clearly depicts that F(ab′)$_2$4.1 is not saturated with DOTA and more sites are available for modification. One to two DOTA attachments per F(ab′)$_2$4.1 are desired as it was previously demonstrated that Gd-DTPA modification of another contrast agent with more than one Gd-DTPA moiety per molecule adversely affected its BBB permeability (22).

Polyamine and DOTA Modified F(ab′)$_2$4.1. After DOTA conjugation, the protein was modified with the polyamine putrescine using the carbodiimide reaction. The

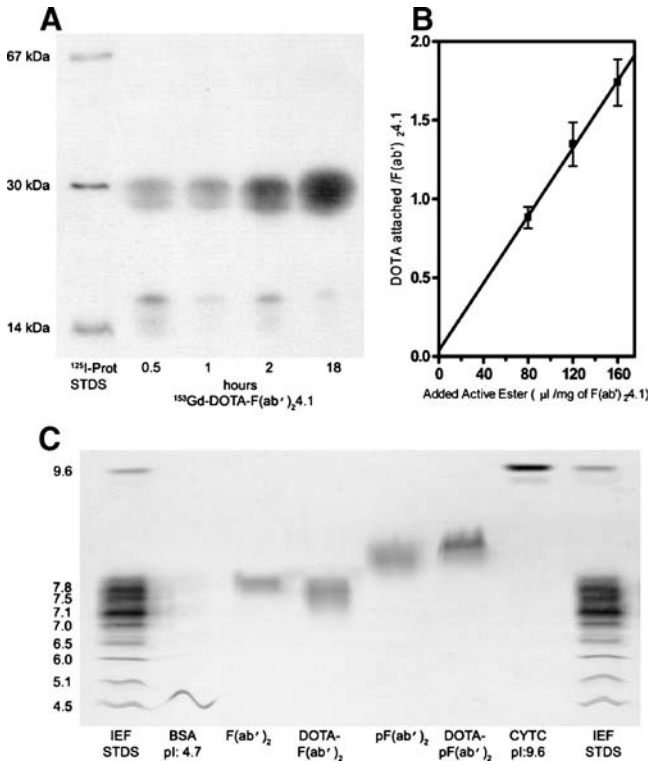

Fig. 1. **A** Autoradiography of the time course study of DOTA coupling reaction with F(ab′)$_2$4.1 detected by chelation with ^{153}Gd followed by SDS-PAGE under reduced condition. ^{125}I Prot STDS - α-lactoalbumin 14 KDa; Carbonic anhydrase 30 KDa; Albumin 67 KDa. **B** DOTA coupling to F(ab′)$_2$4.1 evaluated by paper chromatography. The *abscissa* plots the amount of active ester added in microliter per milligram of F(ab′)$_2$4.1, and the ordinate plots the number of DOTA attached per F(ab′)$_2$4.1. **C** Isoelectric focusing of F(ab′)$_2$4.1 and DOTA-F(ab′)$_2$4.1 fragments before and after polyamine modification. *IEF STDS* Broad-range IEF standards, *BSA* bovine serum albumin, *CYTC* cytochrome C.

polyamine modification involves the conversion of carbodiimide activated carboxyl groups of protein into primary amino groups by 1,4-diaminobutane (putrescine). The extent of this reaction depends largely on the pH and the availability of the carboxyl groups. Previously we have demonstrated the protein p*I* dependence of polyamine modification of F(ab′)$_2$4.1, where the decrease in pH of the reaction increases the degree of polyamine modification of the protein followed by a progressive decrease in its antigen binding ability (14). IgG4.1 has a neutral p*I* (~6.8) and the F(ab′)$_2$4.1 has a p*I* of 7.9, whereas, the completely polyamine modified F(ab′)$_2$4.1 has a basic p*I* of ~9.7 (14). Similarly, the DOTA and polyamine-modified F(ab′)$_2$4.1 showed a shift in the isoelectric point to a more basic p*I*, demonstrating modification of the carboxylic acid groups on the protein with the polyamine (Fig. 1C). Complete modification of DOTA-F(ab′)$_2$4.1 with the polyamine was demonstrated, therefore no further chromatographic purification was necessary to separate DOTA-pF(ab′)$_2$4.1 from any residual unmodified DOTA-F(ab′)$_2$4.1 protein.

ELISA of IgG4.1 and F(ab′)$_2$4.1 Derivatives With and Without Gd-DOTA Polyamine Modifications. Figure 2 shows the ELISA binding of soluble and fibrillar form of Aβ40 and Aβ42 to IgG4G8, IgG4.1, F(ab′)$_2$4.1 derivatives with and without Gd-DOTA and polyamine modifications. IgG4G8 was used as a positive control, which binds to amino acid residues 17–24 of Aβ40/42 peptide. As shown in Fig. 2A–D, F(ab′)$_2$4.1 showed greater binding to soluble and fibrillar forms of Aβ40 and Aβ42 compared to Gd-DOTA-pF(ab′)$_2$4.1. Gd-DOTA-pF(ab′)$_2$4.1 showed relatively better binding compared to the whole IgG4.1 and IgG4G8 with soluble Aβ40/42 (Fig. 2A,B). With fibrils, however, they all showed comparable binding (Fig. 2C,D). When IgG specific whole antibody molecule was used as the secondary antibody for the ELISA experiment, IgG4.1 and IgG4G8 showed enhanced binding to soluble Aβ40 compared to the F(ab′)$_2$4.1 fragments (data not shown). The non-specific L227 antibody which was used a negative control did not show any binding to Aβ40–42 peptides (data not shown).

Plasma Pharmacokinetics of ^{125}I-F(ab′)$_2$4.1 and ^{125}I-Gd-DOTA-pF(ab′)$_2$4.1. Plasma concentration profiles over a

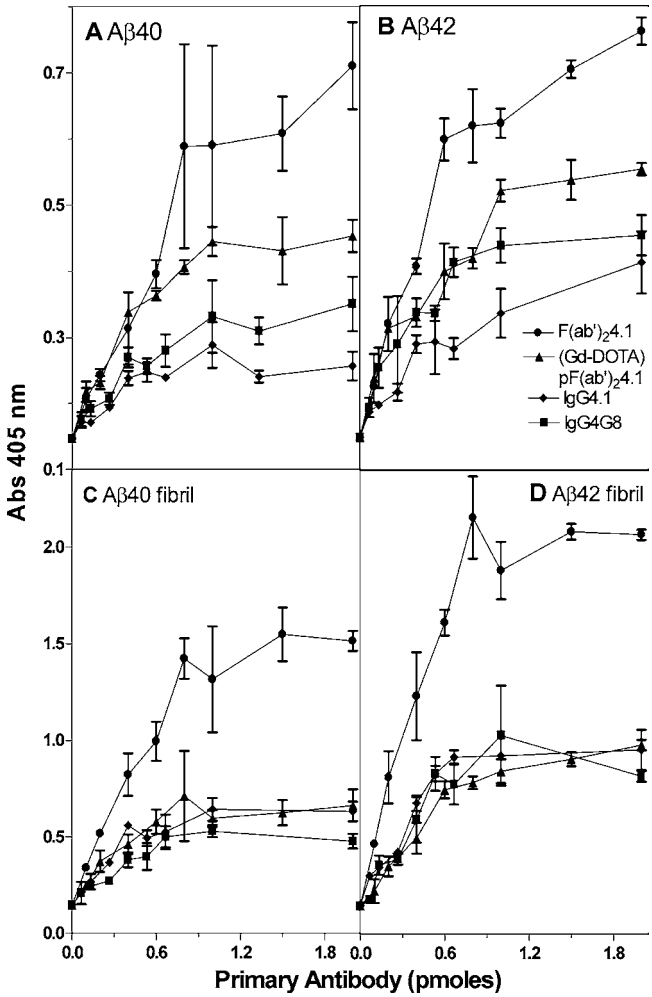

Fig. 2. ELISA binding of soluble and fibrillar Aβ40 and Aβ42 to F(ab′)$_2$4.1, Gd-DOTA- pF(ab′)$_2$4.1, IgG4.1, and IgG4G8. Anti-Aβ standard antibody 4G8 was used as positive control. Fab specific antibody was used as a secondary antibody. However, when IgG specific whole antibody was used, IgG4.1 and IgG4G8 showed enhanced binding to soluble Aβ40 compared to the F(ab′)$_2$4.1 fragments (data not shown). The *abscissa* plots the amount of primary antibody in picomoles per well from 0 to 2 pmol. The *ordinate* plots the absorbance at 405 nm.

course of time for ^{125}I-F(ab′)$_2$4.1 and ^{125}I-Gd-DOTA-pF(ab′)$_2$4.1 were fitted by the function: $C(t)=Ae^{-\alpha t}+Be^{-\beta t}$, where $C(t)$ is the amount (μCi) of ^{125}I-F(ab′)$_2$4.1 or ^{125}I-Gd-DOTA-pF (ab′)$_2$4.1 per 1 ml of plasma; A and B are the intercepts, and α and β are the slopes of the curve. This biexponetial fit was determined adequate based on Akaike information criterion, Schwartz criterion, *F*-test, and by the visual examination of the residual plots.

The plasma clearance (CL) of ^{125}I-Gd-DOTA-pF(ab′)$_2$4.1 is significantly higher than ^{125}I-F(ab′)$_2$4.1, which is reflected in the lower plasma levels of ^{125}I-Gd-DOTA-pF(ab′)$_2$4.1 compared to ^{125}I-F(ab′)$_2$4.1 (Fig. 3A). Moreover, the α and β half-lives of ^{125}I-Gd-DOTA-pF(ab′)$_2$4.1 were substantially lower than that of ^{125}I-F(ab′)$_2$4.1, resulting in lower C_{max} and AUC values (Table I). Similarly the polyamine modified F(ab′)$_2$4.1 has a rapid plasma clearance and much lower α and β half-lives than the Gd-DOTA-pF(ab′)$_2$4.1. The accumulation of these compounds are greater in the kidney compare to the liver and spleen (Fig. 3B). While pF(ab′)$_2$4.1 has a greater accumulation in the kidney, the Gd-DOTA-pF(ab′)$_2$4.1 has nearly five fold lower accumulation in the kidney.

BBB Permeability of Radioiodinated Contrast Agent. The contrast agent was radioiodinated with ^{125}I/^{131}I and the permeability coefficient×surface area product (PS×10^{-6} milliliters per gram per second) and residual blood volume (V_p in microliters per gram) were determined (Table II). The contrast agent had PS values ranging from 27 to 58×10^{-6} ml g^{-1} s^{-1} in six different brain regions of mice, where as the unmodified F(ab′)$_2$4.1 had PS values from 1 to 2×10^{-6} ml g^{-1} s^{-1}, which showed 18–33 fold higher BBB permeability for the contrast agent compared to the native F(ab′)$_2$4.1. The V_p values were not significantly different between the contrast agent and F(ab′)$_2$4.1. The high PS value of the contrast agent indicates high BBB permeability which may facilitate its delivery at the blood brain barrier to target amyloid plaques in APP/PS1 mouse brain. Interestingly, addition of ~2 DOTA molecules per F(ab′)$_2$4.1 did not decrease the BBB permeability of the molecule compared to polyamine modified F(ab′)$_2$4.1 without Gd-DOTA, which is attributed to the relative smaller size of DOTA compared to the much larger F(ab′)$_2$4.1 molecule.

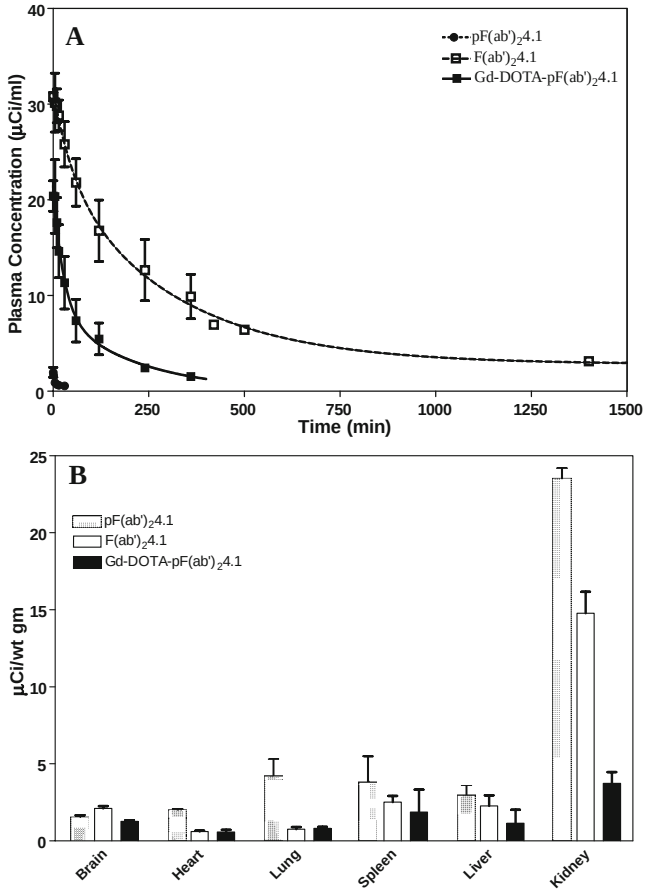

Fig. 3. Plasma pharmacokinetics (**A**), and biodistribution (**B**) of ^{125}I-pF(ab′)$_2$4.1, ^{125}I- F(ab′)$_2$4.1, ^{125}I-Gd-DOTA-pF(ab′)$_2$4.1 in 6 month old WT mice.

Labeling of Amyloid Plaques In Vitro. ^{125}I-IgG4.1, ^{125}I-F(ab′)$_2$4.1, ^{125}I-Gd-DOTA-F(ab′)$_2$4.1, ^{125}I-pF(ab′)$_2$4.1, and ^{125}I-Gd-DOTA-pF(ab′)$_2$4.1 were tested *in vitro* with APP/PS1 mouse brain sections to determine their ability to bind amyloid plaque deposits in APP/PS1 double transgenic mouse. All of them labeled amyloid plaques and deposits in APP/PS1 mouse brain sections *in vitro* (Fig. 4). The antibody fragment, F(ab′)$_2$4.1, labeled amyloid deposits to a similar level as compared to the intact immunoglobulin, IgG4.1, in APP/PS1 mouse sections (Fig. 4C and B, respectively). The polyamine and gadolinium-modified versions of F(ab′)$_2$4.1, particularly the putative contrast agent, Gd-DOTA-pF(ab′)$_2$4.1, also labeled amyloid plaques in the mouse brain sections (Fig. 4D–F).

In Vivo Targeting. ^{125}I-F(ab′)$_2$4.1, ^{125}I-Gd-DOTA-pF(ab′)$_2$4.1, or a non-specific mouse monoclonal antibody were injected IV into APP/PS1 mice to determine the ability of the gadolinium and polyamine modified fragment to label amyloid deposits within the brain. The amyloid deposits were stained using a rabbit polyclonal anti-Aβ antibody and immunohistochemical methods while the presence of the radiolabeled immunoglobulins was detected by emulsion microautoradiography with exposure times of 1, 2, and 4 weeks (for 4 week exposure see Fig. 5). Labeling, demonstrated by high densities of exposed (black) silver grains, could be observed for all three immunoglobulins on the brain sections after 1 week of exposure. The pattern of labeling was much different for the three immunoglobulins. The labeling of F(ab′)$_2$4.1 and the non-specific antibody was observed predominantly in blood vessels and blood vessel walls (i.e., arrowheads, Fig. 5A, C). The non-specific antibody did not label amyloid plaques. Labeled amyloid plaques were observed occasionally for F(ab′)$_2$4.1. These were limited to small, isolated clusters of labeled deposits in close proximity to a blood vessel (i.e., arrows, Fig. 5C and D). Most amyloid plaques, however, were not labeled by F(ab′)$_2$4.1. The gadolinium and putrescine-modified fragment, Gd-DOTA-pF(ab′)$_2$, however, exhibited labeling of amyloid deposits throughout the parenchyma of the brain, particularly the cortex and hippocampus (Fig. 5E and F). This is most likely due to the higher permeability of Gd-DOTA-pF(ab′)$_2$ at the BBB. These results demonstrate that Gd-DOTA-pF(ab′)$_2$

Table I. Plasma Pharmacokinetic Parameter Estimates for ^{125}I-F(ab′)$_2$4.1 and ^{125}I-Gd-DOTA-pF(ab′)$_2$4.1

Parameters	Units	^{125}I-pF(ab′)$_2$4.1	^{125}I-F(ab′)$_2$4.1	^{125}I-Gd-DOTA-pF(ab′)$_2$4.1
Maximum plasma concentration (C_{max})	μCi/ml	2.093±0.019	31.04±0.48	21.52±0.76***[a], **[b]
Coefficient (A)	μCi/ml	1.389±0.0292	19.22±2.36	13.20±2.99**[b]
Coefficient (B)	μCi/ml	0.704±0.0307	11.81±2.43	8.31±3.14*[b]
Distribution rate constant (α)	1/min	0.369±0.0225	0.009±0.002	0.037±0.012***[a], ***[b]
Elimination rate constant (β)	1/min	0.008±0.002	0.001±0.0003	0.005±0.002
Area under the curve (AUC)	min×μCi/ml	95.57±21.20	13431±2093	2130±383**[a], **[b]
Clearance (CL)	ml/min	1.046±0.232	0.0074±0.001	0.0469±0.0084**[a], **[b]

The data is expressed as mean±SEM.
*p<0.05, **p<0.01, and ***p<0.001
[a] Comparing ^{125}I-F(ab′)$_2$4.1 with ^{125}I-Gd-DOTA-pF(ab′)$_2$4.1
[b] Comparing ^{125}I-pF(ab′)$_2$4.1 with ^{125}I-Gd-DOTA-pF(ab′)$_2$4.1

crosses the BBB and labels amyloid plaques *in vivo* after a single IV bolus injection.

Incubation of Gd-DOTA-pF(ab′)$_2$4.1 with APP Mouse Brain Slices In Vitro for MR Imaging of Contrast Enhanced Amyloid Plaques. Gd-DOTA-pF(ab′)$_2$4.1 was incubated with unfixed APP transgenic mouse brain slices to test the ability of Gd-DOTA-pF(ab′)$_2$4.1 to bind amyloid plaques and provide plaque specific contrast enhancement for MRI. Representative images from the MRI scans are illustrated in Fig. 6. The T_1- weighted spin echo (T_1SE) image in Fig. 6A shows many hyperintense foci (bright spots) throughout the cortex and hippocampus. Many of these hyperinstense foci matched the hypointense foci (dark spots) in the T_2-weighted spin echo (T_2SE) image in Fig. 6C by anatomical spatial co-registration using linked-cursor image analysis software (Analyze®) (23). These hypointense foci are not present in T_2SE images of non-transgenic, wild-type mice, which also do not exhibit amyloid plaques. While hypointense foci can be observed in T_2SE image of AD mouse brain in Fig. 6D, no hyperintense foci (bright spots) were observed in T_1SE images shown in Fig. 6B in the absence of a gadolinium modified contrast enhancing agent. Plaques appear as dark spots on T_2SE images because they contain iron. Since iron is a paramagnetic species, it causes local magnetic susceptibility resulting in decreased signal intensity. We have previously shown that most of the hypointense foci (dark spots) observed in T_2SE images of AD mouse brain can be spatially co-registered to Thioflavin *S*-positive amyloid plaques in histologically stained sections (6,11,25). Gadolinium is a commonly-used MRI contrast enhancing agent that accelerates relaxation in T_1SE scans. Therefore, the presence of hyperintense foci in the T_1SE image that also spatially co-register with hypointense foci on the T_2SE image indicates that the Gd-DOTA-pF(ab′)$_2$4.1 not only labeled amyloid plaques in the APP mouse brain slice, but also caused plaque-specific selective contrast enhancement in the T_1SE MR image.

DISCUSSION

The present studies demonstrates that Gd-DOTA-pF(ab′)$_2$4.1 showed nearly 30 fold increase in BBB permeability compared to the unmodified F(ab′)$_2$4.1, binds specifically to amyloid plaques, and produces local changes in tissue

Table II. PS and V_p Values of F(ab′)$_2$4.1, pF(ab′)$_2$4.1 and Gd-DOTA-pF(ab′)$_2$4.1 at the BBB in the WT Mouse

				pF(ab′)$_2$4.1 *vs.* F(ab′)$_2$4.1		Gd-DOTA-pF(ab′)$_2$4.1 *vs.* F(ab′)$_2$4.1		Gd-DOTA-pF(ab′)$_2$4.1 *vs.* pF(ab′)$_2$4.1	
	F(ab′)$_2$4.1[a]	pF(ab′)^{2}4.1[a]	Gd-DOTA-pF(ab′)$_2$4.1	RI	P*	RI	P*	RI	P*
PS (ml g^{-1} s^{-1} ×10^6)									
Cortex	1.2±0.1	33.3±1.5	38.8±1.7	27.8	<0.001	32.3	<0.001	1.2	NS
Caudate-putamen	1.2±0.1	39.1±5.0	26.8±1.2	32.6	<0.001	22.3	<0.001	0.7	NS
Hippocampus	1.5±0.2	49.9±8.2	48.0±2.2	33.3	<0.001	32.0	<0.001	1.0	NS
Thalamus	1.7±0.2	35.7±3.0	42.7±1.9	21.0	<0.001	25.1	<0.001	1.2	NS
Brainstem	2.2±0.1	41.2±2.6	57.8±2.6	18.7	<0.001	26.3	<0.001	1.4	NS
Cerebellum	1.9±0.2	64.7±4.1	56.0±2.5	34.1	<0.001	29.5	<0.001	0.9	NS
*V*p (μl/g)									
Cortex	18.8±1.2	20.4±2.5	24.8±6.5	1.1	NS	1.3	NS	1.2	NS
Caudate-putamen	11.8±1.0	13.0±1.3	13.8±4.3	1.1	NS	1.2	NS	1.1	NS
Hippocampus	19.8±2.7	18.8±1.5	32.7±9.6	1.0	NS	1.7	NS	1.7	NS
Thalamus	27.5±1.3	20.7±5.1	27.0±7.9	1.0	NS	1.4	NS	1.3	NS
Brainstem	27.5±1.4	28.1±6.1	39.0±9.4	1.0	NS	1.4	NS	1.4	NS
Cerebellum	27.9±2.2	30.8±5.8	38.9±10.7	1.1	NS	1.4	NS	1.3	NS

RI Relative increase, *NS* not significant
[a] Data are $\bar{x}$ ±SEM values, n=4 for F(ab′)2, n=3 for pF(ab′)2, n=5 for Gd-pF(ab′)2
*(p>0.05) p by ANOVA

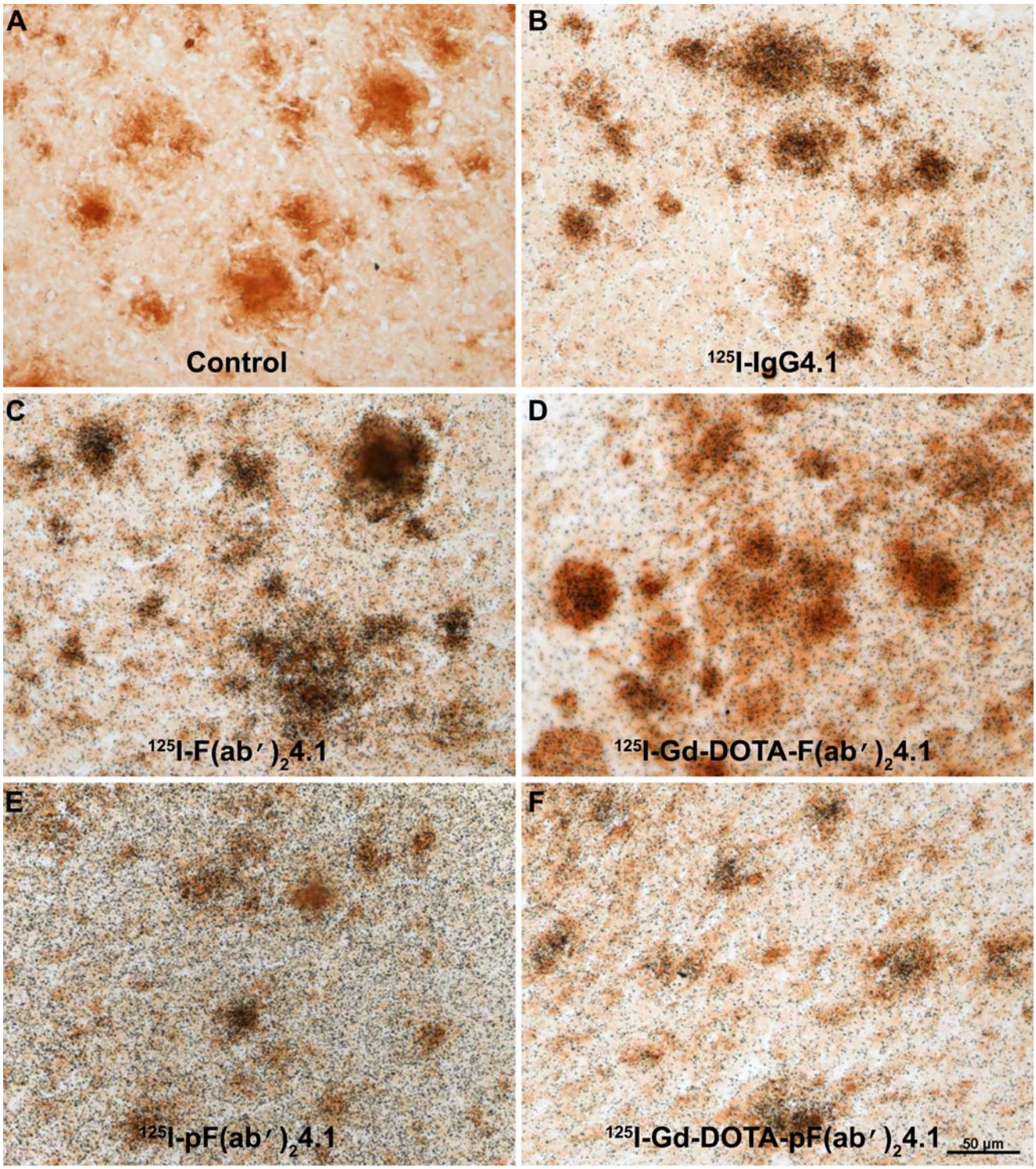

Fig. 4. *In vitro* binding of ^{125}I-IgG4.1 (**B**), ^{125}I-F(ab′)$_2$4.1 (**C**), ^{125}I-Gd-DOTA-F(ab′)$_2$4.1 (**D**), ^{125}I-pF(ab′)$_2$4.1 (**E**), and ^{125}I-Gd-DOTA-pF(ab′)$_2$4.1 (**F**) to amyloid deposits in cortex of AD transgenic mouse brain sections. A control section (**A**) was incubated with PBS alone. Photomicrographs of histological sections processed for anti-Aβ immunohistochemistry with a rabbit polyclonal antibody and emulsion autoradiography with 2 weeks of exposure. *Scale bar*=50 µm.

contrast enhancement with APP transgenic mouse brain slices that are detectable by MRI. In principle, an ideal brain MRI contrast agent for visualizing and quantifying the pathological burden of Aβ plaque deposits should meet the following criteria: (1) have high systemic bioavailability; (2) cross the BBB in sufficient quantities; (3) bind specifically to plaques with high affinity; and (4) produce local changes in tissue contrast that are detectable by MRI.

Since IgG4.1 is an endogenous molecule raised from the mouse immune system, its fragment, F(ab′)$_2$4.1 or covalently modified F(ab′)$_2$4.1, is expected to be stable *in vivo* with high systemic bioavailability. In addition, removal of the Fc

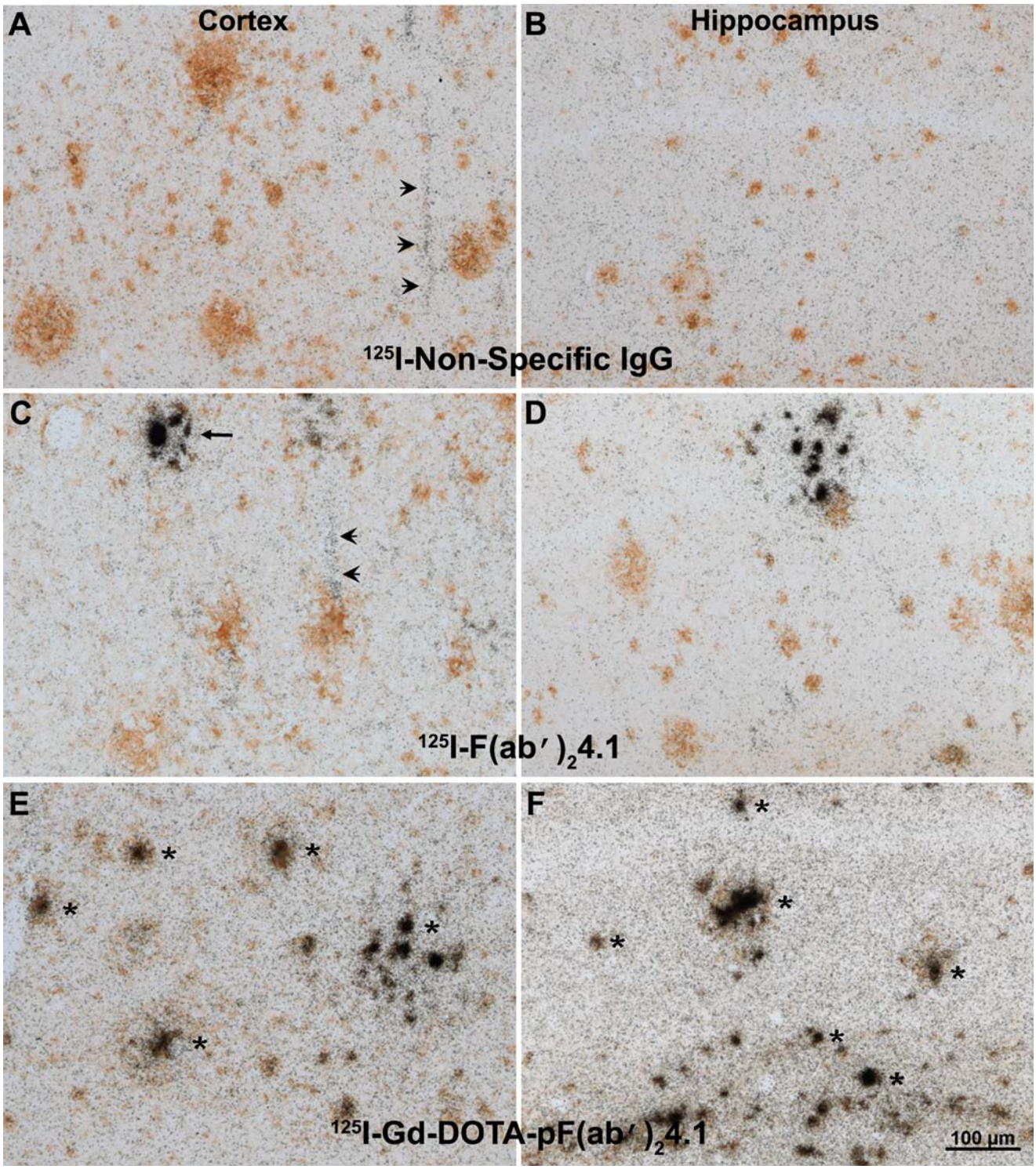

Fig. 5. *In vivo* labeling of amyloid deposits in AD transgenic mouse brain following IV injection of a ^{125}I-labeled non-specific antibody (**A**, **B**), ^{125}I-F(ab′)$_2$4.1 (**C**, **D**), or ^{125}I-Gd-DOTA-pF(ab′)$_2$4.1 (**E**, **F**). Photomicrographs of histological sections processed for anti-Aβ immunohistochemistry with a rabbit polyclonal antibody and emulsion autoradiography with 4 weeks of exposure were taken in cortex (**A**, **C**, **E**) and the CA1 subfield of the hippocampus (**B**, **D**, **F**). *Arrowheads* indicate labeled blood vessels (**A**, **B**, **C**). *Arrows* indicate a small cluster of plaques labeled by ^{125}I-F(ab′)$_2$4.1 in the vicinity of a blood vessel (**C**, **D**). Numerous plaques in cortex and hippocampus were labeled with ^{125}I-Gd-DOTA-pF(ab′)$_2$4.1 (**E**, **F**). A few examples are labeled with *asterisks*. *Scale bar*=100 μm.

portion from IgG4.1 will also minimize the risks associated with the inflammatory response and cerebral hemorrhaging as reported in active and some passive immunotherapy studies (26). Also, because of the larger molecular size, internalization of this probe by cells in the brain parenchyma is expected to be limited so that most of the probe should be available for imaging the amyloid plaques in the extracellular milieu. The use of the cyclic Gd-DOTA chelating complex,

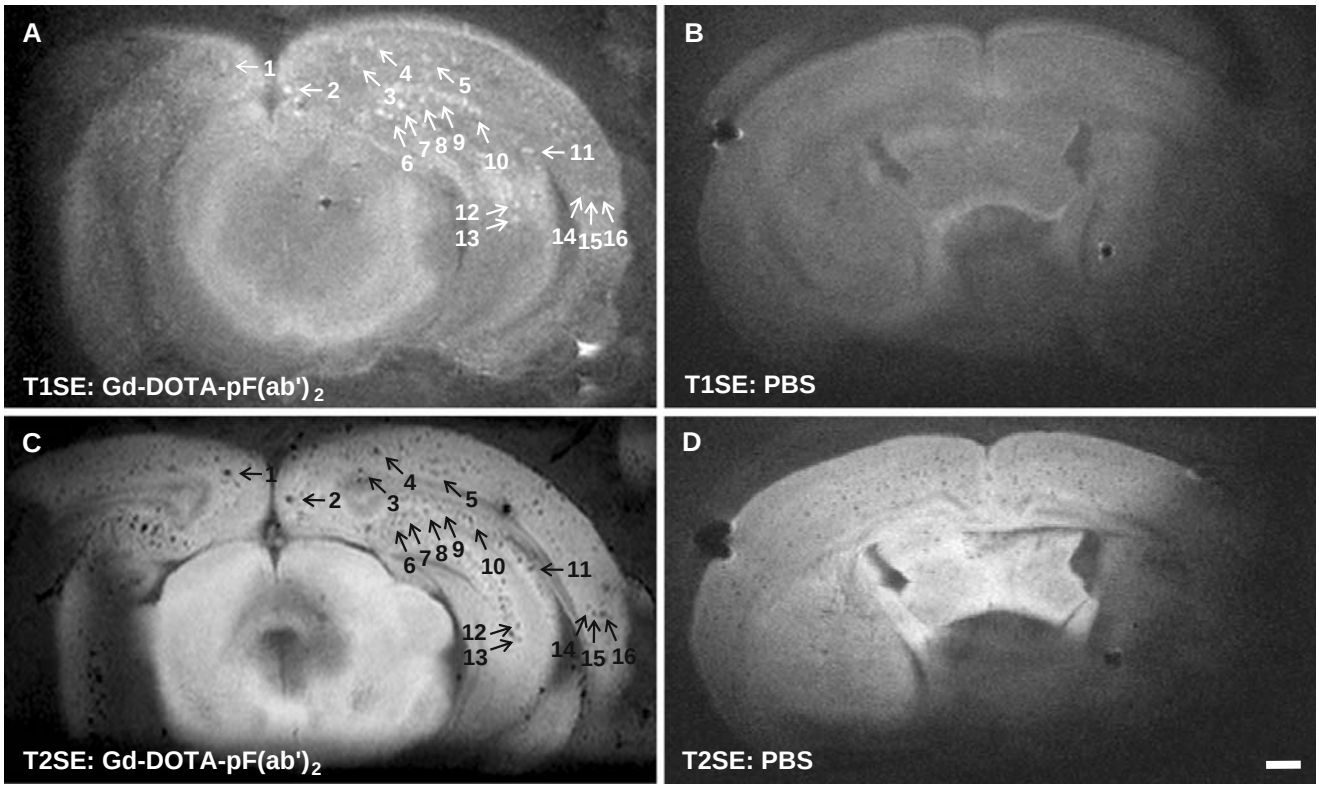

Fig. 6. T_1SE (**A**, **B**) and T_2SE (**C**, **D**) MR images of an APP mouse brain slices incubated with Gd-DOTA-pF(ab′)$_2$4.1 (**A**, **C**) and with PBS alone under (**B**, **D**) *in vitro* condition. Sixteen selective contrast enhanced plaques in cortex and hippocampus confirmed by spatial co-registration are indicated by arrows and numbers. *Scale bar*=500 μm.

which has greater stability compared to the noncyclic Gd-DTPA chelating complex, will allow the tight chelation of Gd to minimize the release of any toxic free Gd ions *in vivo* (17).

When injected intravenously in WT mice, pF(ab′)$_2$4.1 was cleared from the systemic circulation more rapidly compared to F(ab′)$_2$4.1 (Fig. 3A) and primarily accumulated in kidney and liver. The plasma pharmacokinetics of Gd-DOTA-pF(ab′)$_2$4.1 revealed some interesting trends. The plasma residence time of Gd-DOTA-pF(ab′)$_2$4.1 was significantly higher than that of pF(ab′$_2$4.1. In addition Gd-DOTA-pF(ab′)$_2$4.1 showed decreased accumulation in the kidney and liver compare to pF(ab′)$_2$4.1 and even F(ab′)$_2$4.1 (Fig. 3B). These pharmacokinetic features are characteristic of cationized proteins, such as, rapid elimination from the systemic circulation and significant distribution to tissues, which adds to the safety of the contrast agent, because it has been reported cationized proteins that rapidly accumulate in the kidney pose potential renal toxicity (27,28).

Based on the ELISA, the binding epitopes of F(ab′)$_2$4.1 were largely preserved during the synthesis of Gd-DOTA-pF (ab′)$_2$4.1 by employing careful conditions used for the two step carbodiimide reaction. The binding of Gd-DOTA-pF (ab′)$_2$4.1 to Aβ fibrils is comparable to that of the whole antibody IgG4.1 and IgG4G8 when a Fab specific secondary antibody was used in the ELISA experiment, but somewhat less than that of native F(ab′)$_2$4.1. Similar effects were also observed in the *in vitro* binding experiments of radioiodinated Gd-DOTA-pF(ab′)$_2$4.1, which showed somewhat fewer silver grains compared to the radioiodinated F(ab′)$_2$4.1 with APP/PS1 mouse brain slices. However, when radioiodinated Gd-DOTA-pF(ab′)$_2$4.1 was injected intravenously into APP/PS1 mice, it labels amyloid plaques *in vivo* in different regions of the cortex and hippocampus. This labeling was highly specific to amyloid plaques, whereas radioiodinated nonspecific IgG label was only found in blood vessels and not the amyloid plaques. The *in vivo* labeling of radioiodinated Gd-DOTA-pF (ab′)$_2$4.1 clearly demonstrated that it crossed the BBB and labeled amyloid plaques present in the APP/PS1 brain parenchyma.

Furthermore, incubation of Gd-DOTA-pF(ab′)$_2$4.1 with the brain slices of an APP mouse followed by MRI showed selective enhancement of plaques on the T_1-weighted spin echo MR image. Contrast-enhanced amyloid plaques were visible throughout the cortex and hippocampus of the brain. Many of the bright spots seen in the T_1SE MR image, which are from the T_1 relaxation of Gd present in the contrast agent, are matched with the dark spots of T_2SE MR image of the same brain slice. Previously Poduslo et al. (6) demonstrated that the dark spots observed in T_2SE images of AD mouse brain were spatially co-registered with Thioflavin S-positive amyloid plaques. These experiments demonstrate that Gd-DOTA-pF(ab′)$_2$4.1 binds to amyloid plaques and the chelated Gd through the covalent linkage of DOTA shows plaque-specific selective contrast enhancement in T_1SE image

This is not the first report of using antibodies as imaging agents to detect amyloid plaques. Majocha et al. (29) developed a murine monoclonal antibody against the first 28 amino acids of the Aβ peptide for the potential imaging of amyloid angiopathy in AD. They enzymatically cleaved the antibody to Fab fragments and labeled it with ^{99m}Tc for in vitro autoradiography assessment after incubation with AD brain sections. These Fab fragments labeled amyloid present

in the blood vessels of AD brain slices under *in vitro* condition. Further development of the probe for *in vivo* studies were not possible because it did not cross the BBB (30). Lee et al. (31) developed a rat monoclonal antibody against mouse transferrin receptor that was complexed to radioiodinated Aβ40 using the metabolically stabile biotin-streptavidin linkage. The intent here was to use the transferrin receptor at the BBB to deliver Aβ, which would bind to the amyloid plaques. Subsequent *ex vivo* autoradiographic analysis of AD mouse brain slices suggested bulk tissue enhancement of this complex with the whole brain slice showing extensive silver grain deposition. No mention was made of animal perfusion after IV injection, so it is not clear how successful this antibody complex was delivered across the BBB. The inability to cross the BBB in sufficient quantities could be a major limitation for the failure of these probes to be used as a putative contrast agent.

While polyamine modification of macromolecules to increase the permeability at the BBB has been our strategy, other promising approaches were also reported in the literature. Recently, Kumar et al. (32) successfully targeted siRNA to the brain neuronal cells across the BBB using a short peptide derived from rabies viral glycoprotein coupled with nine arginine (positively charged) residues. Several positively charged cell-penetrating peptides covalently coupled with protein were also used to enable as a cargo to cross the BBB [see review Patel et al. (33)]. In another study, Boado et al. (34) developed a trifunctional fusion protein with three functionalities. The first one is the engineered monoclonal antibody against the human insulin receptor which triggers the receptor mediated transcytosis from blood to brain across the BBB, the second one is engineered single chain variable fragments from antibody raised against the Aβ peptide—to bind and disaggregate the amyloid plaques of AD. The third functionality is Fc receptor of human antibody to cause the reverse transcytosis. While the mechanism of each delivery could be different, the successful brain delivery largely relies on targeting drugs in sufficient quantities across the BBB. Those limits could be higher for a diagnostic probe and may be lower for the therapeutic probe. About 30–40 fold increase in the permeability of polyamine modified macromolecules at the BBB may be closer to the minimum threshold limit to see some positive physiological response.

Additionally to validate this molecular probe as a potential MRI contrast agent to detect AD in live animals or patients depends on several other factors, including optimizing the pharmacokinetics and delivery routes of Gd-DOTA-pF(ab′)$_2$4.1 administration to increase its bioavailability; evaluating the minimum dosage required for amyloid plaque detection; and developing improved MRI pulse sequences to image contrast enhanced plaques *in vivo*. This study highlights the potential of the polyamine modification, which mediates the delivery of radioiodinated Gd-DOTA-pF(ab′)$_2$4.1 to the AD mice brain across the BBB as demonstrated by *in vivo* immunohistochemistry. The molecular probe also binds to amyloid plaques and shows a selective amyloid plaque specific contrast enhancement in T_1SE MR image under *in vitro* conditions. In principle, the delivery approach described here might also be applicable to the delivery of other diagnostic or therapeutic proteins for various neurological disorders.

ACKNOWLEDGEMENTS

The authors would like to thank Dr. Karen Duff for the PS1 transgenic mouse line, Dawn Gregor for her expert technical assistance, and Dr. Thomas G. Beito and Dr. Chella S. David of the Mayo Monoclonal Core Facility. Thanks to Prof. Shawn Que Hee, director of ICP-MS facility for the ICP-mass spectral analysis. Support was provided by the Neuroscience Cores for MR Studies of the Brain from NINDS (NS057091) and the Minnesota Partnership for Biotechnology and Medical Genomics.

REFERENCES

1. D. J. Selkoe. Clearing the brain's amyloid cobwebs. *Neuron*. **32**:177–180 (2001).
2. W. E. Klunk, H. Engler, A. Nordberg, Y. M. Wang, G. Blomqvist, D. P. Holt, M. Bergstrom, I. Savitcheva, G. F. Huang, S. Estrada, B. Ausen, M. L. Debnath, J. Barletta, J. C. Price, J. Sandell, B. J. Lopresti, A. Wall, P. Koivisto, G. Antoni, C. A. Mathis, and B. Langstrom. Imaging brain amyloid in Alzheimer's disease with Pittsburgh Compound-B. *Ann. Neurol*. **55**:306–319 (2004).
3. N. P. Verhoeff, A. A. Wilson, S. Takeshita, L. Trop, D. Hussey, K. Singh, H. F. Kung, M. P. Kung, and S. Houle. *In-vivo* imaging of Alzheimer disease beta-amyloid with [11C]SB-13 PET. *Am. J. Geriatr. Psychiatry*. **12**:584–595 (2004).
4. G. W. Small, V. Kepe, L. M. Ercoli, P. Siddarth, S. Y. Bookheimer, K. J. Miller, H. Lavretsky, A.C. Burggren, G.M. Cole, H.V. Vinters, P.M. Thompson, S.C. Huang, N. Satyamurthy, M.E. Phelps, and J.R. Barrio. PET of brain amyloid and tau in mild cognitive impairment. *N. Engl. J. Med*. **355**:2652–2663 (2006).
5. C. R. Jack, T. M. Wengenack, D. A. Reyes, M. Garwood, G. L. Curran, B. J. Borowski, J. Lin, G. M. Preboske, S. S. Holasek, G. Adriany, and J. F. Poduslo. *In vivo* magnetic resonance microimaging of individual amyloid plaques in Alzheimer's transgenic mice. *J. Neurosci*. **25**:10041–10048 (2005).
6. J. F. Poduslo, T. M. Wengenack, G. L. Curran, T. Wisniewski, E. M. Sigurdsson, S. I. Macura, B. J. Borowski, and C. R. Jr Jack. Molecular targeting of Alzheimer's amyloid plaques for contrast-enhanced magnetic resonance imaging. *Neurobiol. Dis*. **11**:315–329 (2002).
7. Y. Z. Wadghiri, E. M. Sigurdsson, M. Sadowski, J. I. Elliott, Y. S. Li, H. Scholtzova, C. Y. Tang, G. Aguinaldo, M. Pappolla, K. Duff, T. Wisniewski, and D. H. Turnbull. Detection of Alzheimer's amyloid in Transgenic mice using magnetic resonance microimaging. *Magn. Reson. Med*. **50**:293–302 (2003).
8. H. Benveniste, G. Einstein, K. R. Kim, C. Hulette, and G. A. Johnson. Detection of neuritic plaques in Alzheimer's disease by magnetic resonance microscopy. *Proc Natl Acad Sci U S A*. **96**:14079–14084 (1999).
9. J. A. Helpern, S. P. Lee, M. F. Falangola, V. V. Dyakin, A. Bogart, B. Ardekani, K. Duff, C. Branch, T. Wisniewski, M. J. de Leon, O. Wolf, J. O'Shea, and R. A. Nixon. MRI assessment of neuropathology in a transgenic mouse model of Alzheimer's disease. *Magn. Reson. Med*. **51**:794–798 (2004).
10. G. Vanhoutte, I. Dewachter, P. Borghgraef, F. Van Leuven, and A. Van der Linden. Noninvasive *in vivo* MRI detection of neuritic plaques associated with iron in APP[V717I] transgenic mice, a model for Alzheimer's disease. *Magn Reson Med*. **53**:607–613 (2005).
11. C. R. Jr Jack, M. Garwood, T. M. Wengenack, B. Borowski, G. L. Curran, J. Lin, G. Adriany, O. H. Grohn, R. Grimm, and J. F. Poduslo. *In vivo* visualization of Alzheimer's amyloid plaques by magnetic resonance imaging in transgenic mice without a contrast agent. *Magn. Reson. Med*. **52**:1263–1271 (2004).
12. J. F. Poduslo, G. L. Curran, and C. T. Berg. Macromolecular Permeability across the Blood–Nerve and Blood–Brain Barriers. *Proc. Natl. Acad. Sci. U S A*. **91**:5705–5709 (1994).

13. J. F. Poduslo, and G. L. Curran. Amyloid beta peptide as a vaccine for Alzheimer's disease involves receptor-mediated transport at the blood–brain barrier. *Neuroreport*. **12**:3197–3200 (2001).
14. J. F. Poduslo, M. Ramakrishnan, S. S. Holasek, M. Ramirez-Alvarado, K. K. Kandimalla, E. J. Gilles, G. L. Curran, and T. M. Wengenack. *In vivo* targeting of antibody fragments to the nervous system for Alzheimer's disease immunotherapy and molecular imaging of amyloid plaques. *J. Neurochem*. **102**:420–433 (2007).
15. L. Holcomb, M. N. Gordon, E. McGowan, X. Yu, S. Benkovic, P. Jantzen, K. Wright, I. Saad, R. Mueller, D. Morgan, S. Sanders, C. Zehr, K. O'Campo, J. Hardy, C. M. Prada, C. Eckman, S. Younkin, K. Hsiao, and K. Duff. Accelerated Alzheimer-type phenotype in transgenic mice carrying both mutant amyloid precursor protein and presenilin 1 transgenes. *Nature Med*. **4**:97–100 (1998).
16. K. Hsiao, P. Chapman, S. Nilsen, C. Eckman, Y. Harigaya, S. Younkin, F. S. Yang, and G. Cole. Correlative memory deficits, A beta elevation, and amyloid plaques in transgenic mice. *Science*. **274**:99–102 (1996).
17. P. M. Smith-Jonesand, and D. B. Solit. Generation of DOTA-conjugated antibody fragments for radioimmunoimaging. *Methods Enzymol*. **386**:262–275 (2004).
18. U. K. Laemmli. Cleavage of structural proteins during the assembly of the head of bacteriophage T4. *Nature*. **227**:680–685 (1970).
19. J. F. Poduslo, G. L. Curran, T. M. Wengenack, B. Malester, and K. Duff. Permeability of proteins at the blood–brain barrier in the normal adult mouse and double transgenic mouse model of Alzheimer's disease. *Neurobiology of Disease*. **8**:555–567 (2001).
20. J. B. Bassingthwaighte, F. P. Chinard, C. Crone, C. A. Goresky, N. A. Lassen, R. S. Reneman, and K. L. Zierler. Terminology for mass transport and exchange. *Am. J. Physiol*. **250**:H539–545 (1986).
21. J. F. Poduslo, G. L. Curran, T. M. Wengenack, B. Malester, and K. Duff. Permeability of proteins at the blood–brain barrier in the normal adult mouse and double transgenic mouse model of Alzheimer's disease. *Neurobiol Dis*. **8**:555–567 (2001).
22. J. F. Poduslo, G. L. Curran, J. A. Peterson, D. J. McCormick, A. H. Fauq, M. A. Khan, and T. M. Wengenack. Design and chemical synthesis of a magnetic resonance contrast agent with enhanced *in vitro* binding, high blood–brain barrier permeability, and *in vivo* targeting to Alzheimer's disease amyloid plaques. *Biochem*. **43**:6064–6075 (2004).
23. R. A. Robb. A software system for interactive and quantitative analysis of biomedical images. In K. H. F. Hohne, and S. M. Pizer (eds.), *3D Imaging in Medicine*. Springer, Berlin, 1990, pp. 333–361.
24. M. Marjanska, G. L. Curran, T. M. Wengenack, P. G. Henry, R. L. Bliss, J. F. Poduslo, C. R. Jr Jack, K. Ugurbil, and M. Garwood. Monitoring disease progression in transgenic mouse models of Alzheimer's disease with proton magnetic resonance spectroscopy. *Proc. Natl. Acad Sci. U S A*. **102**:11906–11910 (2005).
25. C. R. Jr Jack, T. M. Wengenack, D. A. Reyes, M. Garwood, G. L. Curran, B. J. Borowski, J. Lin, G. M. Preboske, S. S. Holasek, G. Adriany, and J. F. Poduslo. *In vivo* magnetic resonance microimaging of individual amyloid plaques in Alzheimer's transgenic mice. *J. Neurosci*. **25**:10041–10048 (2005).
26. Y. Tamura, K. Hamajima, K. Matsui, S. Yanoma, M. Narita, N. Tajima, K. Q. Xin, D. Klinman, and K. Okuda. The F(ab′)2 fragment of an Abeta-specific monoclonal antibody reduces Abeta deposits in the brain. *Neurobiol. Dis*. **20**:541–549 (2005).
27. P. Bergmann, R. Kacenelenbogen, and A. Vizet. Plasma clearance, tissue distribution and catabolism of cationized albumins with increasing isoelectric points in the rat. *Clin Sci (Lond)*. **67**:35–43 (1984).
28. W. M. Pardridge. Strategies for drug delivery through the blood–brain barrier. *Neurobiol Aging*. **10**:636–637 (1989)(discussion 648–650).
29. R. E. Majocha, J. M. Reno, R. P. Friedland, C. VanHaight, L. R. Lyle, and C. A. Marotta. Development of a monoclonal antibody specific for beta/A4 amyloid in Alzheimer's disease brain for application to *in vivo* imaging of amyloid angiopathy. *J. Nucl Med*. **33**:2184–2189 (1992).
30. R. P. Friedland, J. Shi, J. C. Lamanna, M. A. Smith, and G. Perry. Prospects for noninvasive imaging of brain amyloid beta in Alzheimer's disease. *Ann. N Y Acad Sci*. **903**:123–128 (2000).
31. H. J. Lee, Y. Zhang, C. Zhu, K. Duff, and W. M. Pardridge. Imaging brain amyloid of Alzheimer disease *in vivo* in transgenic mice with an Abeta peptide radiopharmaceutical. *J.Cereb.Blood Flow Metab*. **22**:223–231 (2002).
32. P. Kumar, H. Wu, J. L. McBride, K. E. Jung, M. H. Kim, B. L. Davidson, S. K. Lee, P. Shankar, and N. Manjunath. Transvascular delivery of small interfering RNA to the central nervous system. *Nature*. **448**:39–43 (2007).
33. L. N. Patel, J. L. Zaro, and W.C. Shen. Cell penetrating peptides: intracellular pathways and pharmaceutical perspectives. *Pharm Res*. **24**:1977–1992 (2007).
34. R.J. Boado, Y. Zhang, C. F. Xia, and W. M. Pardridge. Fusion antibody for Alzheimer's disease with bidirectional transport across the blood–brain barrier and abeta fibril disaggregation. *Bioconjug Chem*. **18**:447–455 (2007).